Composition effect on the aggregate/solution interface of a nematic lyotropic liquid crystal

Article *in* RSC Advances · January 2016

DOI: 10.1039/C6RA13597H

6 authors, including:

Jose Javier Lopez Cascales
Universidad Politécnica de Cartagena
64 PUBLICATIONS **884** CITATIONS
SEE PROFILE

Ramiro Araya-Maturana
Universidad de Talca
107 PUBLICATIONS **530** CITATIONS
SEE PROFILE

F. Guillermo Díaz Baños
University of Murcia
53 PUBLICATIONS **568** CITATIONS
SEE PROFILE

Composition effect on the aggregate/solution interface of a nematic lyotropic liquid crystal.

A.R. Ruiz-Fernández[†,‡], J.J. López-Cascales[‡,*], J.J. Giner-Casares[Ⓢ], R. Araya-Maturana[§], F.G. Díaz-Baños[£], and B.E. Weiss-López[†,*]

August 17, 2016

† Universidad de Chile, Facultad de Ciencias, Departamento de Química, Casilla 653, Santiago, Chile.
Ⓢ CIC biomaGUNE, Biofunctional Nanomaterials - Laboratory 6 Parque tecnológico de San Sebastián, Ed. Miramón 182, Guipúzcoa, 20009 Donostia - San Sebastián, Spain
‡ Universidad Politécnica de Cartagena, Grupo de Bioinformática y Macromoléculas (BioMac), Area de Química Física Aulario II, Campus de Alfonso XIII, 30203 Cartagena, Murcia, Spain.
§ Universidad de Talca, Instituto de Química de Recursos Naturales, Casilla 747, Talca, Chile.
£ Uni. de Murcia, Fac. de Química, Dep. de Química Física, Campus de Espinardo, 30100 Espinardo, Murcia, Spain.

* To whom correspondence should be addressed: javier.lopez@upct.es and bweiss@uchile.cl.

Abstract

Lyotropic nematic liquid crystals (lnlc) have attracted attention due to their resemblance with natural membranes and several technological applications. The effect of tetradecyltrimethyl amonium chloride (TTAC) in the viscosity of a new lnlc containing also decanol, NaCl and natural lipids, was studied. In this article we study how the concentration of phospholipids, decanol and NaCl affects the bilayer and the liquid crystal/solution interface structures. ^{2}H-NMR quadrupole splittings and longitudinal relaxation times of several deuterated species were measured. Polarized light microscopy, transmission electron microscopy and kinematic viscosity were also obtained. The structure of the bilayer is dominated by the surface charge density of TTAC. Water rotation, translation and ion solvation, depend on the charge and distance from the interface. Increasing TTAC, MD predicts hydrocarbon chain inter-digitation and lipid rafts formation. This was rationalized using energy arguments.

1 Introduction

Different lyotropic liquid crystalline phases result from the self-assembly of amphiphilic molecules, such as lipids and surfactants in water, when their concentration achieve a certain value, because of hydrophobic and electrostatic interactions.[1–4] In this context, water plays a crucial role regulating the forces that drive the formation of these molecular aggregates. Different properties such as ^{2}H-NMR quadrupole splittings ($\Delta\nu_q$) and longitudinal relaxation times (T_1), water re-orientation, translational diffusion coefficient and ions solvation, among others, can be modified by changes in the composition of the aggregate/solvent interface. For instance, different types of water molecules, in terms of their physicochemical properties, are expected in the solution, depending on their distance from the interface, and it is very likely that the structure of the bilayer itself is also affected by its composition.

A new nematic lyotropic liquid crystal formed by tetradecyltrimethyl amonium chloride (TTAC), decanol (DeOH), sodium dodecyl sulphate (SDS), sodium chloride (NaCl) and a natural mixture of lipids extracted from soybean (PL), constituted mostly by phosphatidylcholine (DOPC) and phosphatidylethanolamine (POPE), all dissolved in water, has been previously prepared. This nematic liquid crystal shows that variations of about 30% w/w in TTAC content continuously increases the magnitude of the viscosity by more than 24 times, making them suitable for certain biomedical applications as lubricants for artificial implants in hips, shoulders and knees, and certain therapies against osteo-arthritis or rheumatoid-arthritis diseases.[5] Therefore, since the effects of TTAC content on the structure and dynamics of the aggregate itself were already studied,[5] in this work we explore the consequences of introducing variations in DeOH, PL and NaCl content, on the structures of the bilayer and the interface. $\Delta\nu_q$ and T_1 from DHO and $\Delta\nu_q$ from DeOH-α-d_2, were measured to explore the dynamics near the interface, mainly to locate the phase transitions. $\Delta\nu_q$ and T_1 from DHO and SDS-d_{25} were measured in selected samples, to probe the dynamics at the interface and towards the interior of the hydrophobic core. Transmission electron microscopy (TEM) and polarized light microscopy (PLM) images of representative compositions were also obtained. Because the structure of the molecular aggregates that form the liquid crystal appears to be very dependent on the surface charge density provided by TTA^+, here we study how it affects solvent properties going from the interface to the bulk aqueous solution. Effectively, water dynamic properties such as diffusion coefficient, rotational correlation time and ions solvation, were obtained from previously simulated trajectories. To validate the molecular dynamics simulations, T_1 of DHO were measured and the results compared with values obtained from simulation. Finally, effects of variations in TTAC composition on the structures of the bilayer and interface, were examined as well.

2 Materials and Methods

2.1 Mesophase Preparation

TTAC, SDS, SDS-d_{25}, D_2O, DeOH and the PL mixture were purchased from Aldrich. Water of HPLC grade and NaCl at 99.8% purity were purchased from Merck. All reagents were used as received.

DeOH-α-d_2 was synthesized by reduction of ethyl decanoate esther with $LiAlD_4$ and purified by vacuum distillation. 5% w/w D_2O was added to the solvent to provide ^{2}H-NMR signal from DHO. For a detailed characterization of the dynamics towards the interior of the hydrophobic core, SDS was replaced by SDS-d_{25} in selected samples.

In order to explore concentration effects on the interface properties, from components not studied before, we have prepared three series of samples, one for DeOH, one for PL and a third series extending the range of NaCl concentration. Consequently, a series of 4 samples containing 0.2253 mg TTAC, 0.0912 mg NaCl, 0.0481 mg DeOH, 0.012 mg SDS and 0.0466, 0.0816, 0.1165 and 0.1400 mg PL, were dissolved in 1 ml of water each. Similarly, a second series of 4 samples containing 0.1165 mg PL, 0.2253 mg TTAC, 0.0912 mg NaCl, 0.012 mg SDS and 0.0351, 0.0442, 0.0506 and 0.0547 mg of DeOH was also prepared. Finally, a third series of 4 samples containing 0.1165 mg PL, 0.2253 mg TTAC, 0.0481 mg DeOH, 0.012 mg SDS and 0.0623, 0.0771, 0.0912 and 0.1070 mg NaCl each, was also prepared. All mentioned samples contained DeOH-α-d_2 and D_2O. Selected samples, representative of the different phases found, were reproduced by using DeOH and SDS-d_{25} instead of DeOH-α-d_2 and SDS.

Before any measurement was performed, all mesophases were allowed to equilibrate at least 48 hours at either 300 K or 298 K, for NMR or kinematic viscosity (η), respectively.

2.2 ^{2}H-NMR Spectra

All NMR spectra were registered using a Bruker Avance 400 NMR spectrometer, located at the Universidad de Santiago de Chile, employing a broadband probe tuned to 61.425 MHz. The ^{2}H 90° pulse was 19 μs long and more than 1000 transients from a spectral window of 40 kHz were accumulated in 32 kB files. T_1 were obtained using the standard T1IR experiment.

2.3 Polarized Light Microscopy (PLM) and Kinematic Viscosity (η)

A Motic series B microscope equipped with crossed polarizers was used to obtain the textures. To orient the aggregates, the samples were mounted in a concave

glass microscope and exposed to a 1.4 T magnet for 15 minutes; more time in the magnet does not modify the textures. Photographs were obtained at 300 K, along the direction of the field, with a 20-fold magnification, from the center of the concavity, to assure that all textures arise from the same sample thickness.

Kinematic viscosities of the solutions, η, were measured using a standard Ubbelohde viscometer at 298 K and 1 atmosphere.

2.4 Transmission Electron Microscopy

TEM images were collected with a JEOL JEM-1400PLUS instrument operating at 120 kV, using carbon coated 400 square mesh copper grids. Samples were drop casted onto the TEM grids. All TEM images were obtained in conditions identical to those previously reported.[5]

2.5 Molecular Dynamics Calculations

GROMACS package 4.5.3 was used to calculate the molecular dynamics trajectories, and most of the analysis of this work, were carried out using our own code. The integration time step was 4 fs. Van der Waals forces were simulated using the Lennard Jones potential (LJ), and electrostatic interactions were calculated with the Particle Mesh Ewald (PME) method.[6,7] In both cases, a cut-off of 1.2 nm was employed. The bond lengths were restrained using LINCS.[8] All simulations were carried out in a NPT ensemble at 300 K and 1 atm, coupled to weak temperature and pressure baths algorithms,[9] with time constants of 0.1 ps and 1 ps for temperature and pressure, respectively. The Ryckaert-Belleman potential[10] was used in all torsions along the aliphatic chains, for a better reproduction of cis-trans transitions. Simple Point Charge (SPC)[11] was the water model considered in all simulations. Atom numeration and charges distribution, can be found elsewhere.[5]

Finally, since most properties of the aggregate depend on the surface charge from TTA^+, a series of calculations employing previously reported trajectories of different systems were performed. The calculated trajectories correspond to experimental samples containing 0.2253 g/ml TTAC (system 1), 0.295 g/ml TTAC (system 2) and 0.2253 g/ml TTAC including 1M NaCl (system 3).

3 Results and Discussion

3.1 Interface Composition

In order to modify the composition of the interface, PL, DeOH and NaCl content were modified and the splittings from DeOH-α-d_2 and DHO measured. The results of these experiments are displayed in Figure 1 of the Supplementary Information (SI). These experiments were performed mainly to locate the compositions

at which the characteristic spectrum of the nematic anisotropic liquid crystal is lost, unequivocal sign that the mesophase was destroyed. Once these limits have been identified, samples representative of the different nematic mesophases found were prepared incorporating SDS-d_{25}, to probe the order and dynamics, not only at the interface, but also towards the interior of the hydrophobic core.[12] Figure 1 show the ^{2}H-NMR spectra from SDS-d_{25} and DHO, Figure 2 display the PLM textures and Figure 3 corresponds to TEM images arising from selected samples. Figures 1A, 2A and 3A were reproduced from a previous work.[5] Measured values of $\Delta\nu_q$ and T_1 from SDS-d_{25} and DHO are presented in table 1, and values of η for these samples are listed in table 2.

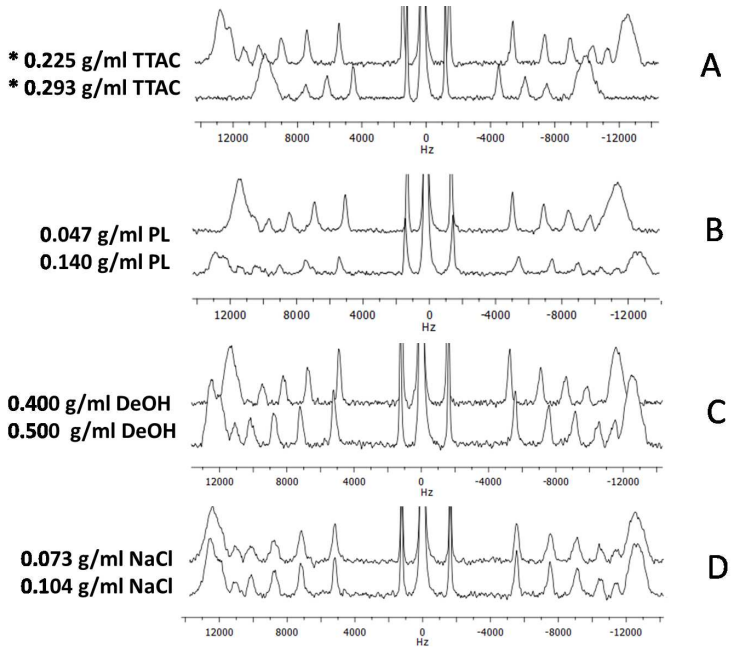

Figure 1: ^{2}H-NMR spectra from SDS-d_{25} and DHO of selected samples. * Previously reported results.[5]

An inspection to table 1 reveals that, as expected, $\Delta\nu_q$ is greater for the first CD_2 of the chain and decreases towards the interior of the bilayer. It is also observed that increasing the content of either PL or DeOH, both have the same effect on $\Delta\nu_q$ and T_1 of SDS-d_{25}, the first increases and the second decreases, for all deuterium atoms towards the interior of the aggregate. This indicates that the degree of alignment of the aliphatic chains with the magnetic field increases and, consequently, their re-orientational dynamics becomes slower. This trend is opposite to that observed when increasing TTAC,[5] and is very likely to arise from a charge screening and spacing effects experienced by the TTA^+ head-groups present at the interface, when increasing the concentration of non-charged amphiphiles.

.	* 0.225 g/ml TTAC		* 0.293 g/ml TTAC		0.047 g/ml PL		0.140 g/ml PL	
Carbon	$\Delta\nu_q(Hz)$	$T_1(ms)$	$\Delta\nu_q(Hz)$	$T_1(ms)$	$\Delta\nu_q(Hz)$	$T_1(ms)$	$\Delta\nu_q(Hz)$	$T_1(ms)$
1	25371	34.2	20153	45.9	22966	40.4	25792	35.4
2	25371	34.2	20153	45.9	22966	40.4	25792	35.4
3	25371	34.2	20153	45.9	22966	40.4	25792	35.4
4	25371	34.2	20153	45.9	22966	40.4	25792	35.4
5	25371	34.2	20153	45.9	22966	40.4	25792	35.4
6	25371	34.2	20153	45.9	22966	40.4	25792	35.4
7	22734	36.7	20153	45.9	22966	40.4	22812	38.7
8	20750	50.2	17386	45.9	19432	66.9	20988	43.3
9	18016	61.5	15054	69.5	16907	76.3	18101	56.2
10	14815	81.9	12371	186.8	13890	94.7	14919	71.7
11	10852	112.4	9046	120.4	10106	125.6	10893	103.4
12	2889	308.3	2383	309.9	2635	352.1	28885	289.4
DHO	18.8	338.9	28.7	317.7	5.8	365.5	26.2	331.4
.	0.040 g/ml DeOH		0.050 g/ml DeOH		0.073 g/ml NaCl		* 0.104 g/ml NaCl	
Carbon	$\Delta\nu_q(Hz)$	$T_1(ms)$	$\Delta\nu_q(Hz)$	$T_1(ms)$	$\Delta\nu_q(Hz)$	$T_1(ms)$	$\Delta\nu_q(Hz)$	$T_1(ms)$
1	23142	37.9	25269	33.4	24983	34.6	25232	31.1
2	23142	37.9	25269	33.4	24983	34.6	25232	31.1
3	23142	37.9	25269	33.4	25232	34.6	25232	31.1
4	23142	37.9	25269	33.4	24983	34.6	25232	31.1
5	23142	37.9	25269	33.4	24983	34.6	25232	31.1
6	23142	37.9	25269	33.4	24983	34.6	24489	31.1
7	21182	41.2	22482	33.9	22468	33.5	22564	36.7
8	20988	54.6	20714	41.9	20562	50.3	20663	42.2
9	18101	59.0	17980	56.1	17831	58.5	17951	52.1
10	14919	75.3	14779	69.2	14689	80.3	14710	70.0
11	10893	111.9	10809	109.1	10723	110.3	10772	99.1
12	2888	289.5	2883	313.2	2865	307.4	2854	294.4
DHO	23.5	337.0	24.5	339.5	28.1	329.8	18.9	334.8

Table 1: Experimental values of ^{2}H-NMR quadrupole splittings ($\Delta\nu_q$, Hz) and longitudinal relaxation time (T_1,ms) of SDS-d_{25} and DHO from selected samples.* Previously reported results.[5]

On the other hand, from Table 2 it is observed that augmenting the content of either PL or DeOH, decreases η by about an order of magnitude, in both cases. This is presumably because the aggregates become smaller. In effect, an increase of either DeOH or PL appears to be equivalent to a decrease in TTAC content, which according with previous results,[5] decreases the size of the aggregate. This makes sense if we observe that $\Delta\nu_q$ from DHO increases in both cases. Decreasing the aggregate's size generates a greater interfacial volume, able to accommodate more oriented solvent molecules, increasing the observed DHO splitting. An inspection to table 1 reveals that the increase in DHO splitting is 20.4 Hz for PL and only 1 Hz for DeOH. Calculated radial distribution functions for the solvation of all head-groups (see section 3.3) shows that solvation capability of PL is greater than for DeOH. Effectively, the ratio between the first solvation layer of (DOPC+POPE)/DeOH is 2.1, supporting this interpretation.

Increasing ionic strength does not significantly affect the order and dynamics of the amphiphiles.[5] Despite the above, η decreased to almost one third the orig-

Sample	Viscosity ($mPa \cdot s$)
* 0.225 g/ml TTAC	12.9 ± 0.1
* 0.293 g/ml TTAC	310 ± 4
0.047 g/ml PL	106.7 ± 0.8
0.140 g/ml PL	8.0 ± 0.2
0.040 g/ml DeOH	59.8 ± 0.4
0.050 g/ml DeOH	7.7 ± 0.1
0.073 g/ml NaCl	29.5 ± 0.2
* 0.104 g/ml NaCl	10.3 ± 0.1

Table 2: Kinematic viscosity of selected samples. * Previously reported results.[5]

inal value with the increase in NaCl, presumably because of a size decrease. A plausible explanation arises from the forces involved in the aggregation process. The higher screening of charges at the interface, at higher ionic strenght, allows smaller aggregates to form, since less aliphatic chain association is necessary to balance the electrostatic repulsions.

As previously reported,[5] a TTAC increment of 30% w/w leads to significant differences in SDS-d_{25} ^{2}H-NMR spectrum and solution η. These observations were explained because higher surface charge density from TTA^+ increased repulsions among the head-groups, incrementing the mobility, decreasing the alignment and modifying the values of $\Delta\nu_q$ and T_1. However, to explain the unusual η increment, another phenomenon, related with modifications in the size and structure of the aggregate itself, going from circular mono-axial to larger elliptic bi-axial, was invoked.

PLM images from selected samples (Figure 2) shows the appearance of the same images observed when modifying TTAC content,[5] oily streaks and Schlieren textures, an indication that the previously observed phase transitions are also occurring with variations in the content of the other components of the aggregate. Previously we concluded that it corresponds to structural changes preserving the bilayer arrangement and nematic character, as evidenced by the ^{2}H-NMR spectra. The oily streak texture is characteristic of homeotropic order, more likely to be found in smaller and better aligned aggregates, but is more usually observed in lamellar phases. Schlieren textures are usually found in nematic mesophases.[13] Despite the similarities observed, there is an obvious difference appreciated in Figure 2: Schlieren textures appear at low concentration of either PL or DeOH, however at higher concentrations oily streaks appear. This order is reversed in the case of TTAC. This observation reveals that effectively it is the surface charge density, i.e. the content of TTA^+, which is controlling the morphology of the aggregates, since increasing the concentration of either PL or DeOH appears to be equivalent to decreasing the concentration of TTA^+, inducing the same phase transitions observed before. To provide more experimental evidence of these changes, TEM images of the selected compositions were obtained and they are displayed in

Figure 3. It is possible to observe similar images than those previously obtained when modifying TTAC content, but in reverse order, corroborating the previous hypothesis.

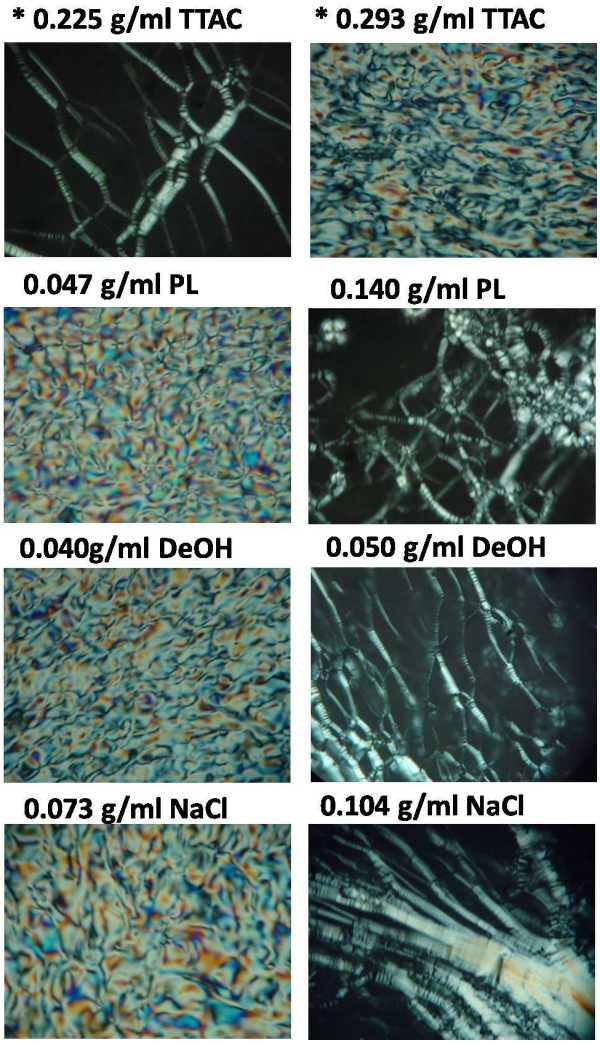

Figure 2: PLM textures of selected samples. * Previously published results.[5]

Since many properties of the aggregate are mostly dependent on the surface charge of TTAC, a detailed theoretical study using previously reported MD trajectories[5] is presented below. As mentioned before, in these simulations a variation in TTAC concentration and ionic strength were introduced. Therefore, the following study is oriented to explore surface charge effects on the bilayer itself, and to reveal how the charge and distance from the surface affects some dynamical properties of the solvent, such as translational diffusion coefficient, rotational correlation time and ions hydration.

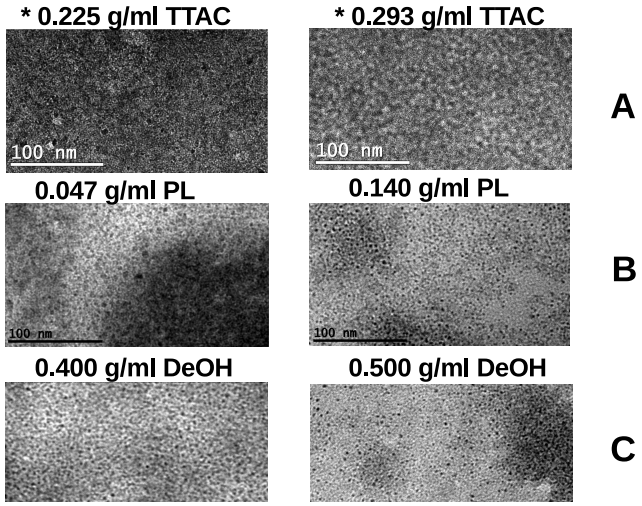

Figure 3: TEM images of selected samples. * Previously published results.[5]

3.2 Rotational Dynamics of Water

To obtain information about the rotational dynamics of the water electric dipole moment near the liquid crystal interface, rotational correlation times at different distances from the center of the bilayer were estimated defining parallel planes of equal thickness at different distances from the interface. Once the thickness of this planes was defined, rotational correlation times were calculated on the basis that each solvent molecule can be assigned to the differents slabs. To do this the 200 ns trayectory lenght was split into sub-trajectories of 20 ps each and the correlation time calculated in each slice. Therefore, from a single trajectory the values going from the interface to the aqueous solution were calculated for systems 1,2 and 3.

In general, water dipole moment re-orientational dynamics can be described by the rotational correlation function which can be formulated in terms of the first Legendre polynomia:

$$< P_1(t) >=< \overrightarrow{\mu(0)}.\overrightarrow{\mu(t)} > \tag{1}$$

where $\overrightarrow{\mu(0)}$ and $\overrightarrow{\mu(t)}$ correspond to the water dipole moment orientation separated by a time interval t.

$< P_1(t) >$ can be fitted to a multi-exponential function, as follows:

$$< P_1(t) >= \sum_{i=1}^{3} a_i e^{\frac{-t}{\tau_i}} \tag{2}$$

here a_i and τ_i correspond to different amplitudes and relaxation times associated with water dipole reorientation.

Since a_i and τ_i are not single valued, a τ_{eff}, independent of the fit, must be defined. Thus, τ_{eff} is defined as follows:[14]

$$\tau_{eff} = \frac{\sum_{i=1}^{3} a_i \tau_i}{\sum_{i=1}^{3} a_i} \tag{3}$$

Figure 4 shows the best fit of $< P_1(t) >$ as a function of time, for different distances from the center of the bilayer, in systems 1 and 2. Thus, from the multi-exponential fit just described, a τ_{eff} at different distances from the interface can be calculated. Figure 5 display τ_{eff} of the water dipole moment for systems 1,2 and 3 as a function of the distance from the center of the bilayer, and shows how it abruptly increases when water approaches the interface. This is due to the fact that water at the interface coordinates the head-group atoms of PL and TTAC, introducing mobility restrictions. From this Figure, we observe how τ_{eff} decreases roughly one order of magnitude when going from the interface to the bulk aqueous solution. However, for the case corresponding to system 2, this increase is less noticeable than in system 1. This decrease in τ_{eff} with the increase in TTAC content, is associated to the relative decrease in PL content, since water coordinates preferentially PL. Hence, a relative decrease in PL content is reflected in a decrease in τ_{eff} as well. System 3 shows a similar behavior as system 1.

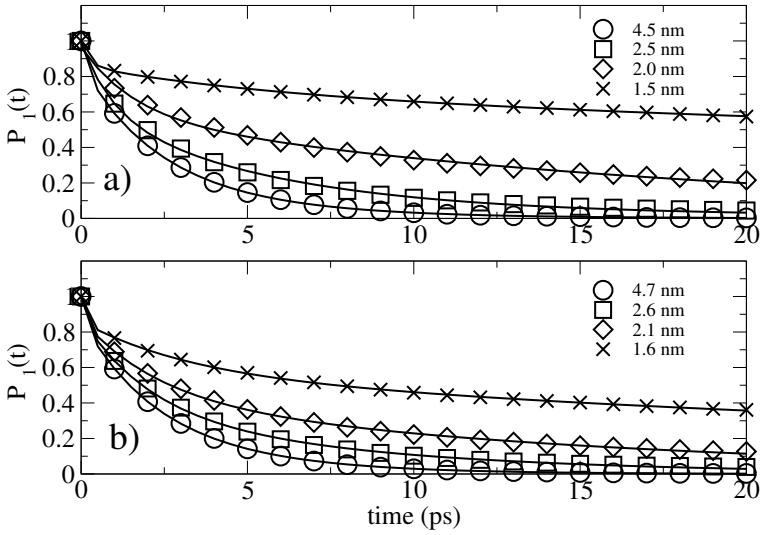

Figure 4: $< P_1(t) >$, as a function of time for (a) system 1 and (b) system 2, at different distances from the center of the bilayer aggregate. Points represent the values obtained from simulation, and solid lines the regression obtained from the multi-exponential fit.

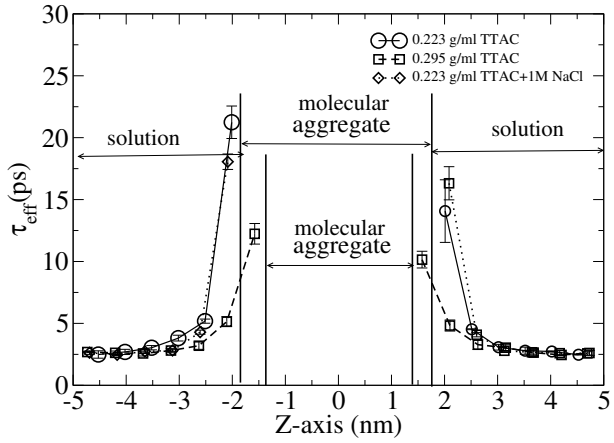

Figure 5: Relaxation time of water dipole moment for the three studied cases, as a function of the distance from the center of the bilayer, $Z = 0$.

To assure that the simulations provide a good representation of the solvent dynamics, T_1 measurements of DHO from samples 1,2 and 3 were carried out and compared with values obtained from simulations. The Redfield theory relates T_1 with the rotational correlation time and the electric field gradient experienced by the nucleus as follows:[15]

$$\frac{1}{T_1} = (\frac{3}{80})(1+\frac{\eta^2}{3})\left[\frac{2\pi eQ}{h}\frac{\partial^2 V}{\partial z^2}\right]^2 (J(\omega_0)+4J(2\omega_0)) \quad (4)$$

where $J(\omega_0)$ is the spectral density. Equation 4 can be evaluated using τ_{eff} calculated above. The electric field gradient is axially symmetric along the $O-D$ bond, ($\eta = 0.00$), the term in square brackets is the quadrupole coupling constant in angular frequency units, 308 kHz for the $O-D$ bond, and ω_0 is the Larmor frequency. Furthermore, assuming that the rotational correlation function is a single exponential decay, the value of T_1 can be easily calculated.[15] T_1 from DHO were measured and values of 339 ms, 318 ms and 334 ms were obteined for samples 1, 2 and 3 respectively. These values are in reasonable agreement with the values 290 ms, 265 ms and 270 ms estimated for bulk water in systems 1, 2 and 3 respectively. Therefore, the simulations appear to represent the solvent dynamics reasonably well.

3.3 Translational Diffusion Coefficient of Water, D_t.

Translational diffusion coefficient of water inside a slice in the xy-plane can be calculated from the mean square displacement as follows:

$$\lim_{t\to\infty} < r^2(t) >= 2n \cdot D_t^{xy} \cdot t \tag{5}$$

where n is the number of degrees of freedom, 2 in this case, r^2 is the square displacement parallel to the xy-plane and t is the time. To provide insights into the variations of water translational dynamics when going from the interface plane to the aqueous bulk solution, D_t at parallel planes of equal thickness from the interface were calculated using a metodology similar to that employed in section 3.2. These results are displayed in Figure 6. System 3 did not show differences with system 1 and is not included in the figure.

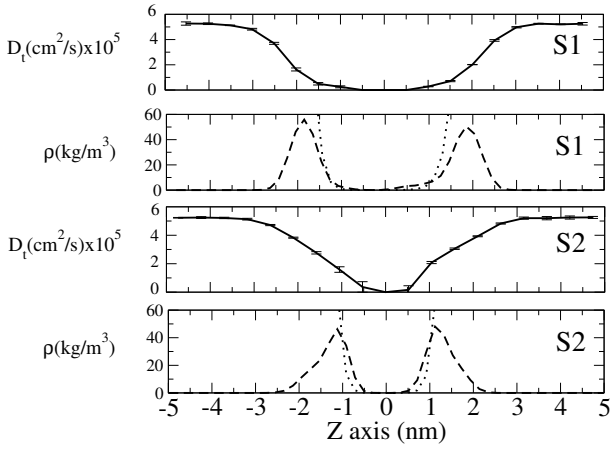

Figure 6: Water translational diffusion coefficient, D_t (solid line), water density (doted line) and TTAC nitrogen distribution (slash line), from bulk water to the interior of the bilayer.(S1) System 1, (S2) System 2.

Figure 6 shows the calculated values of D_t, ranging from about $1.0 \times 10^{-5}\, cm^2 s^{-1}$ near the interfaces to $5.8 \times 10^{-5}\, cm^2 s^{-1}$, at the bulk of the aqueous phase. These values are in agreement with both, experimental and simulation results. In bulk water, $D_t = 7.5 \times 10^{-5}\, cm^2 s^{-1}$ has been reported from the SPC model,[16] and values ranging from $2.3 \times 10^{-5}\, cm^2 s^{-1}$ to $2.74 \times 10^{-5}\, cm^2 s^{-1}$ have been measured using ^{1}H-NMR[17] and ^{2}H-NMR.[18]

At deeper zones of the bilayer interface, water self-diffusion coefficient becomes one fifth the value at the bulk aqueous solution. This decrease is mainly associated to the fact that near the interface, water molecules resembles more solvation water than free water. Furthermore, Figure 6 also shows that there is an important decrease in the width of the hydrophobic core when increasing TTAC, which makes the profiles displayed in Figure 6 significantly different. As previously observed,[5] this reduction has its origin in the inter-digitation of TTAC aliphatic chains when increasing TTAC content and is discussed in section 3.5.

Besides, a study about water coordination around the atoms of PL, DeOH, and TTA^+ head-groups, was performed. The radial distribution function, g(r) is defined by:

$$g(r) = \frac{N(r)}{4\pi r^2 \rho \partial r} \tag{6}$$

here N(r) is the number of atoms in a spherical shell at distance r and thickness ∂r, and ρ is the macroscopic number density, taken as the ratio between the mass of all atoms and the volume of the simulation box. In effect, Figure 7 shows some of these plots and is observed that water is mainly coordinating PL head-groups, and as a consequence, a decrease in the self diffusion coefficient of water in the vicinity of the interface is expected. Head groups of PL and DeOH in system 1 can hold 5.7 and 1.5 water molecules in the first solvation layer, respectively. This values weighted by the mole fraction of each species allowed to estimate the relative degree of solvation. Therefore we can estimate the ratio between the solvation water of PL vs. DeOH to be 2.1. This explains the significant difference observed in the splitting of DHO when increasing either DeOH or PL.

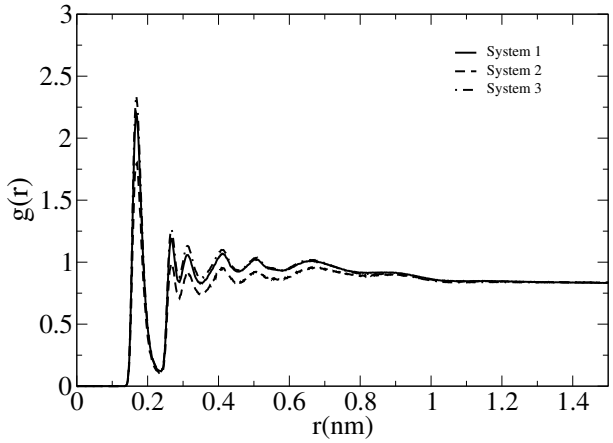

Figure 7: Radial distribution function of water around the phosphate oxygen of DOPC corresponding to systems 1, 2 and 3.

3.4 Sodium and Chloride Hydration Shell

Another aspect related with the stability of the liquid crystal is the structure of ions and the dehydration process when approaching the bilayer/solution interface.

In this regard, a study about the solvation of sodium and chloride ions at different distances from the center of the bilayer, similar to that of sections 3.2 and 3.3, has been performed. From integration of the radial distribution function of water around them, the hydration of these ions can be estimated at the previously defined slabs.

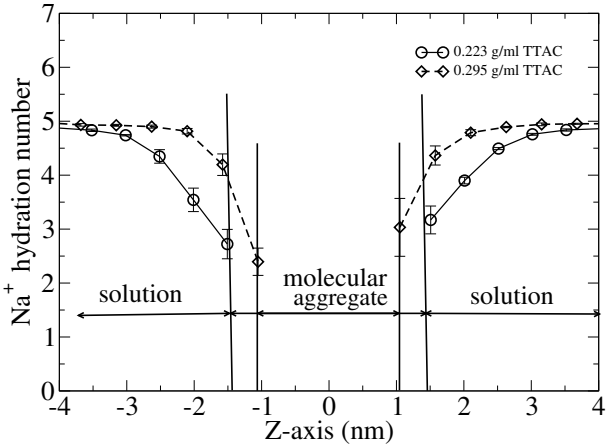

Figure 8: Sodium hydration number from bulk water to deeper zones of the hydrophobic core for two bilayers, corresponding to systems 1 and 2.

Figure 8 shows the results of this study for sodium. Systems 1 and 2 give the same hydration number in the bulk aqueous solution, 5.00 ± 0.02 and 4.90 ± 0.01 respectively. These values agree with the hydration numbers of sodium ions measured by X-ray and from simulations, in which sodium hydration numbers in a range from 4 to 6 water molecules have been reported.[19] Figure 8 also shows how in both cases, a dehydration of almost a 50% takes place for the sodium ions, going from the bulk aqueous solution to the interface.

Figure 9 shows the variation of the chloride hydration number from the bulk aqueous solution to the center of the bilayer, for systems 1 and 2. In bulk solution, hydration numbers of 7.98 ± 0.04 and 8.06 ± 0.03 were obtained for systems 1 and 2 respectively. These values agree with experimental data measured by X-ray,[20] neutron diffraction[21–23] as well as calculated from simulations,[19,24] for which coordination numbers from 5.2 to 7.4 were measured. In all cases studied in this work, counterions completely released their hydration shell when move from bulk water towards the center of the bilayer. Effectively, a variation from 7 water molecules in its hydration state in bulk water to almost naked ions were estimated for chloride when embedded in the middle of the hydrophobic core. Furthermore, Figure 9 also reproduces the reported experimental behavior in which the

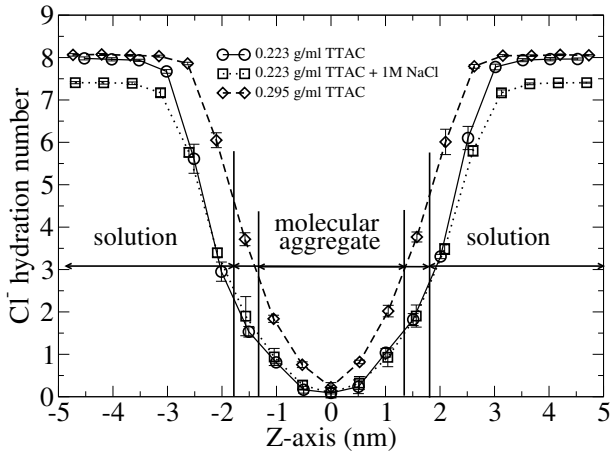

Figure 9: Chloride hydration number from bulk water to the deepest zone of the hydrophobic core for systems 1 and 2.

coordination number decreases with the increase in ionic strength.[25] Thus, from simulation, we obtained a 9% decrease in the chloride hydration number when the salt concentration increased to 1M, following the same behavior than that reported by Cummings et al.,[25] in which a decrease of 11% was measured for the chloride hydration number with the increase in ionic strength. This significant decrease in the hydration shell of chloride ions is compensated by the chloride coordination to the positive charges of TTA^+, as evidenced by the calculated radial distribution function of Cl^- around the TTA^+ (see Figure 2 SI).

3.5 Bilayer Structure

In this section we explore in more detail effects of TTAC content on the structure of the bilayer itself. In this regard, Figure 10 shows the density profiles of TTA^+ across the Z axis, perpendicular to the bilayer surface. It is observed that system 1 shows slightly overlapping hydrocarbon chains, as deduced from the valley located at the center of the plot. This profile contrast with that of system 2, in which a maximum in TTA^+ density is observed at the center of the bilayer. Furthermore, system 2 displays a narrower profile. These observations clearly indicate that inter-digitation of the aliphatic chains of TTA^+ from both leaflets is occurring. This can be understood on the basis of electrostatic and Lennard-Jones interactions. Increasing TTAC content by 30% w/w produces an increment in the ammonium electrostatic repulsions, from 113 kJ/mol to 312 kJ/mol. This is compensated with a better compaction of the hydrocarbon chains, increasing

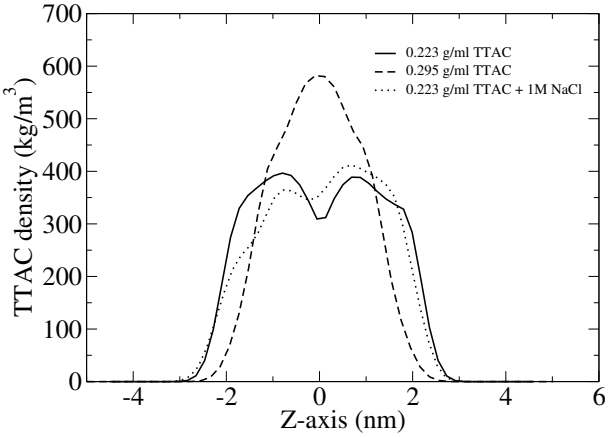

Figure 10: TTAC density across the molecular aggregate for systems 1 and 2. The origin of the z-axis was taken at the center of the bilayer.

TTA^+-TTA^+ Lennard-Jones attractions from -4157 kJ/mol to -6460 kJ/mol.

Furthermore, a visual inspection to the simulated bilayer interfaces reveals the formation of lipid rafts by phospholipids segregation. Figure 11 shows a snapshot of systems 1 after 160 ns simulation and is possible to distinguish the existence of clusters formed by PL only. To provide a thermodynamic explanation for the formation of lipid rafts, we have calculated the potential of mean force (PMF) corresponding to the insertion of DOPC into two ideal systems. Thus, in the first, the insertion of DOPC into a bilayer with a composition identical to system 1, except that all TTAC were removed, was simulated. In the second, DOPC was inserted into a bilayer of TTAC only. The PMF at different depths of the bilayer can be used to estimated the spontaneity of the insertion process in both ideal systems as follows:

$$\Delta G(z) = -RT \ln \frac{c_i(z)}{c_i^0} = PMF \tag{7}$$

Here $\Delta G(z)$ is the difference between the free energy from the bulk aqueous solution to a certain position z, along an axis perpendicular to the bilayer interface. R is the gas constant, T the absolute temperature, $c_i(z)$ the concentration of DOPC at position z, and c_i^0 the concentration of DOPC in the bulk aqueous solution. Due to sampling incompleteness, $c_i(z)$ profiles can not be obtained straightforwardly from normal MD simulations, however, using Umbrella[26] and WHAM[27] methodologies, such as they have been described in previous works,[14,28–30] the PMF associated with the insertion of DOPC into the two systems proposed above was estimated. To improve the sampling, two DOPC molecules were introduced

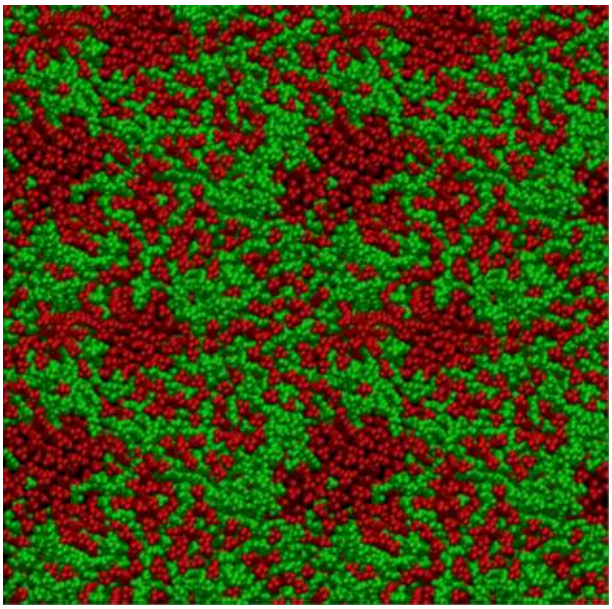

Figure 11: Snapshot of the xy-plane of system 1 after 160 ns of trajectory. Darker areas correspond to clusters of lipids.

into the system, one placed at the bulk water, at a distance of -3.9 nm from the center of the bilayer, and the other placed at the center of the hydrophobic core. Thus, both DOPC molecules were simultaneously shifted 0.1 nm each maintaining a distance of 3.9 nm between them. The motion of the center of mass of each molecule was subjected to a restrain along the z axis using a harmonic potential of $3000N \cdot nm^{-2} \cdot mol^{-1}$, within windows of 0.1 nm thick, but maintaining the freedom of movement in the XY plane. For each of the 40 subsystems, 30 ns of trajectory length were calculated.

Figure 12 shows the PMF associated with the DOPC insertion from bulk water to the interior of the two models described above. This Figure evidences that for any distance along the z axis, DOPC prefers to be surrounded by other DOPC molecules rather than by TTAC. Therefore, according with this result, the formation of lipid rafts in the aggregate is expected, since DOPC shows greater affinity by other phospholipid molecules. Finally, the formation of lipid rafts is favored by about 5 kJ/mol with respect to insertion in a TTA^+ bilayer.

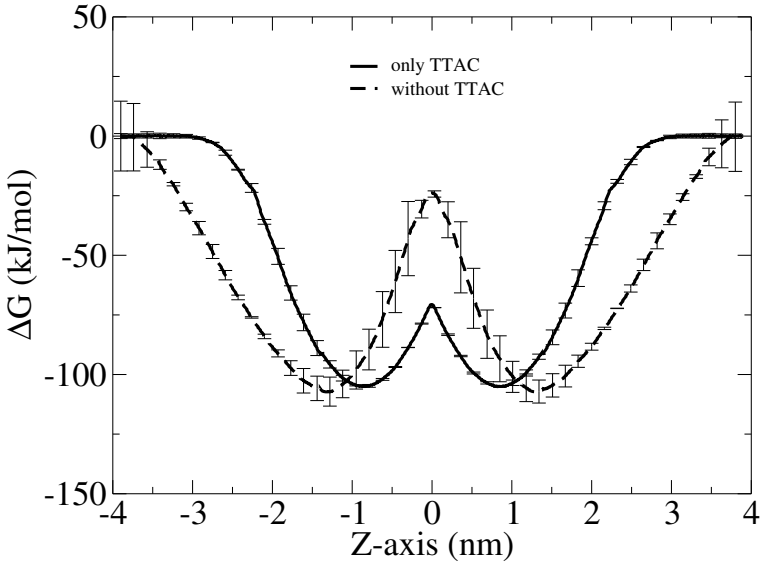

Figure 12: Potential of Mean Force (PMF) associated with the insertion of DOPC from the bulk aqueous solution into the two molecular bilayers mentioned above.

4 Conclusions

The use of MD simulations in the interpretations of the experimental results arising from complex systems, such as lyotropic nematic liquid crystals, has proven to be very useful. In this particular case, the dynamics of the solvent appears to be adequately represented.

All evidence strongly suggest that the surface charge density, provided by TTA^+, is responsible not only for the size and shape of the aggregates, but also has a strong influence in the structure of the bilayer itself, inducing inter-digitation and lipids rafts formation.

Dynamical properties of the solvent, such as translation diffusion coefficient and rotational correlation time, are strongly dependent on the surface charge density and the distance from the interface. This effects disappear at a distance of 3.5 nm away from the interface.

Finally, lipid rafts formation arises from a greater affinity between PL molecules rather than PL-TTA^+.

5 Acknowledgments

The authors are pleased to acknowledge financial support from Fondecyt-Chile (Grant No. 1150138). ARRF acknowledges a fellowship from Conicyt. Authors also acknowledge the Staff of the Computing Center at the Polytechnic University of Cartagena for their support and facilities. JJLC and FGDB acklowledge the financial support from Fundación Séneca (Grants No 19353/PI/14 and 19499/PI/14, respetively). JJGC acknowledges the Ministry of Economy and Competitiveness for a Ramon y Cajal contract (#RyC-2014-14956).

References

[1] C. Tanford, *The Hydrophobic Effect: Formation of Micelles and Biological Membranes 2d Ed*, J. Wiley., 1980.

[2] J. Moreno-Razo, E. Sambriski, N. Abbott, J. Hernandez-Ortiz and J. de Pablo, *Nature*, 2012, **485**, 86–89.

[3] F. Biedermann, W. Nau and H. Schneider, *Angew. Chem. Int. Edit.*, 2014, **53**, 11158–11171.

[4] X. Wang, D. Miller, E. Bukusoglu, J. de Pablo and N. Abbott, *Nat. Mater.*, 2016, **15**, 106–112.

[5] A. Ruiz-Fernández, J. López-Cascales, J. Giner-Casares, R. Araya-Maturana, F. Díaz-Baños, D. Muñoz-Gacitúa and B. Weiss-López, *RSC Adv.*, 2016, **6**, 7455–7464.

[6] T. Darden, D. York and L. Pedersen, *J. Chem. Phys.*, 1993, **98**, 10089–10092.

[7] U. Essmann, L. Perera, M. Berkowitz, T. Darden, H. Lee and L. Pedersen, *J. Chem. Phys.*, 1995, **103**, 8577–8593.

[8] B. Hess, H. Bekker, H. Berendsen and J. Fraaije, *J. Comput. Chem.*, 1997, **18**, 1463–1472.

[9] H. Berendsen, J. Postma, W. van Gunsteren, A. DiNola and J. Haak, *J. Chem. Phys.*, 1984, **81**, 3684–3690.

[10] J. Ryckaert and A. Bellemans, *Faraday Discuss.*, 1978, 95–106.

[11] H. Berendsen, J. Postma, W. van Gunsteren and J. Hermans, *Intermolecular Forces*, D. Reidel Publishing Company, 1981.

[12] M. F. Brown, *J. Magn. Reson.*, 1979, **35**, 203–215.

[13] H. Stegemeyer and H. Behret, *Liquid Crystals*, Steinkopff, 1994.

[14] V. E. Bahamonde-Padilla, J. J. López-Cascales, R. Araya-Maturana, M. Martínez-Cifuentes and B. E. Weiss López, *ChemPhysChem*, 2014, **15**, 1422–1431.

[15] A. Abragam, *Principles of Nuclear Magnetism*, Oxford University Press, 2011, p. 314.

[16] J. López Cascales, J. García de la Torre, S. Marrink and H. Berendsen, *J. Chem. Phys.*, 1996, **104**, 2713–2720.

[17] D. O'Reilly, *J. Chem. Phys.*, 1974, **60**, 1607–1618.

[18] K. Tanaka, *J. Chem. Soc.-Faraday Trans.*, 1974, **71**, 1127–1131.

[19] J. Chandrasekhar, D. Spellmeyer and W. Jorgensen, *J. Am. Chem. Soc.*, 1984, **106**, 903–910.

[20] N. Skipper, S. Cumming, G. Neilson and J. Enderby, *Nature*, 1986, **321**, 52–53.

[21] M. Yamagami, H. Wakita and T. Yamaguchi, *J. Chem. Phys.*, 1995, **103**, 8174–8178.

[22] D. Powell, A. Barnes, J. Enderby, G. Neilson and P. Salmon, *Faraday Discuss.*, 1988, **85**, 137–146.

[23] D. Powell, G. Neilson and J. Enderby, *J. Phys. Condens. Matter*, 1993, **5**, 5723–5730.

[24] J. López Cascales and T. Otero, *J. Chem. Phys.*, 2004, 1951–1957.

[25] S. Cummings, J. Enderby, G. Neilson, J. Newsome, R. Howe, W. Howells and A. Soper, *Nature*, 1980, **23**, 714–716.

[26] G. Torrie and J. Valleau, *J. Comput. Phys.*, 1977, **23**, 187–199.

[27] S. Kumar, D. Bouzida, R. Swensen, P. Kollman and J. Rosemberg, *J. Comput. Chem.*, 1992, **13**, 1011–1021.

[28] J. L. MacCallum and D. P. Tieleman, *J. Am. Chem. Soc.*, 2006, **128**, 125–130.

[29] J. Maccallum, W. Drew Bennett and D. Tieleman, *J. Gen. Physiol.*, 2007, **129**, 371–377.

[30] J. Lopez Cascales, S.D. Oliveira Costa and R. Porasso, *J. Chem. Phys.*, 2011, **135**, 135103–135110.

List of Tables

1 Experimental values of ^{2}H-NMR quadrupole splittings ($\Delta\nu_q$, Hz) and longitudinal relaxation time (T_1,ms) of SDS-d_{25} and DHO from selected samples.* Previously reported results.[5] 7

2 Kinematic viscosity of selected samples. * Previously reported results.[5] 8

List of Figures

1 ^{2}H-NMR spectra from SDS-d_{25} and DHO of selected samples. * Previously reported results.[5] 6

2 PLM textures of selected samples. * Previously published results.[5] 9

3 TEM images of selected samples. * Previously published results.[5] 10

4 $< P_1(t) >$, as a function of time for (a) system 1 and (b) system 2, at different distances from the center of the bilayer aggregate. Points represent the values obtained from simulation, and solid lines the regression obtained from the multi-exponential fit. 11

5 Relaxation time of water dipole moment for the three studied cases, as a function of the distance from the center of the bilayer, $Z = 0$. 12

6 Water translational diffusion coefficient, D_t (solid line), water density (doted line) and TTAC nitrogen distribution (slash line), from bulk water to the interior of the bilayer.(S1) System 1, (S2) System 2. 13

7 Radial distribution function of water around the phosphate oxygen of DOPC corresponding to systems 1, 2 and 3. 14

8 Sodium hydration number from bulk water to deeper zones of the hydrophobic core for two bilayers, corresponding to systems 1 and 2. 15

9 Chloride hydration number from bulk water to the deepest zone of the hydrophobic core for systems 1 and 2. 16

10 TTAC density across the molecular aggregate for systems 1 and 2. The origin of the z-axis was taken at the center of the bilayer. . 17

11 Snapshot of the xy-plane of system 1 after 160 ns of trajectory. Darker areas correspond to clusters of lipids. 18

12 Potential of Mean Force (PMF) associated with the insertion of DOPC from the bulk aqueous solution into the two molecular bilayers mentioned above. 19